Selectivity-Enhancement Technique for Stepped-Impedance-Resonator Dual-Passband Filters

Roberto Gómez-García, *Senior Member, IEEE*, Li Yang, *Member, IEEE*, José-María Muñoz-Ferreras, *Member, IEEE*, and Dimitra Psychogiou, *Member, IEEE*

***Abstract*— A class of stepped-impedance resonator (SIR) dual-band bandpass filter (BPF) with selectivity-enhancement cells is reported. These dual-band filtering cells, which are composed of two open-ended transmission-line segments interconnected at the input, are added at one node of the input and output coupled-line stages. Thus, with regard to the SIR dual-band BPF without cells, they increase the order of each passband by two and simultaneously generate transmission zeros (TZs) at both sides of the two transmission bands. The operating principles of the proposed dual-band BPF are detailed at the coupling–routing-diagram level and design guidelines for its transmission-line configuration are provided. Moreover, for experimental-validation purposes, a 1.57-GHz/2.38-GHz dual-band BPF microstrip prototype with symmetrical absolute bandwidths is manufactured and characterized.**

***Index Terms*— Bandpass filter (BPF), dual-band filter, microstrip filter, planar filter, selectivity-enhancement cell, stepped-impedance resonator (SIR), transmission zero (TZ).**

I. Introduction

THE research on microwave planar multiband bandpass filters (BPFs) has attracted considerable attention during the past few years. Features such as high filtering selectivity through the generation of transmission zeros (TZs) at both sides of all passbands, low in-band insertion loss, compact size, and design flexibility are much desired for them.

A plurality of solutions for planar dual-band BPF designs has been described in the technical literature. For example, the use of dual-resonance resonators [e.g., stepped-impedance resonators (SIRs) [1] or dual-combline resonators [2]] with complex cross-coupling structures for multi-TZ realization, single-mode resonators in split-type arrangements where the spacing between passbands is defined by the bandwidth of the main transmission band that is divided into the two subbands [3], signal-interference topologies [4], and multibehavior resonator schemes with relatively narrow stopband widths [5].

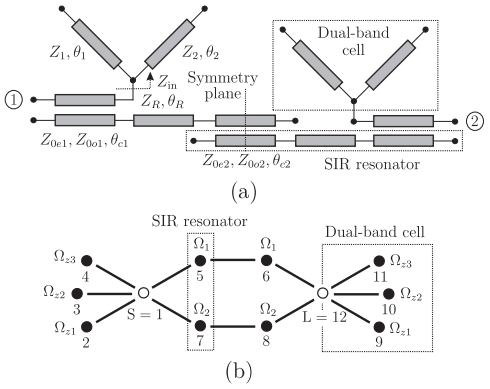

Fig. 1. Proposed SIR-based dual-band BPF with selectivity-enhancement cells—fourth-order example. (a) Circuit details (Z variables: characteristic impedances; Z_{0e} and Z_{0o} variables: even- and odd-mode impedances; θ variables: electrical lengths; and $Z_{in} = 1/Y_{in}$: input impedance of the dual-band cell). (b) Normalized coupling–routing diagram [black circles: resonating nodes; white circles: unitary source (S) and load (L); continuous lines: normalized admittance inverters; Ω_1 and Ω_2: SIR-normalized dual-resonance frequencies; Ω_{z1}, Ω_{z2}, and Ω_{z3}: normalized TZ frequencies].

In this letter, a selectivity-enhancement technique for SIR-based dual-band BPFs is reported. It makes use of dual-band filtering cells that are internally connected at one node of the input and output coupled-line stages to create TZs at both sides of the two overall dual passbands and increase their order, as a benefit with regard to cross-coupling that only produces TZs. The rest of this letter is organized as follows. In Section II, the operational principles and design guidelines of the proposed dual-band BPF with selectivity-increase cells are presented. For practical-validation purposes, a microstrip prototype with fourth-order symmetrical passbands centered at 1.57 and 2.38 GHz is built and tested in Section III. Finally, a summary and the main conclusions of this work are given in Section IV.

II. Theoretical Foundations

A. Operational Principles

The circuit details of the proposed high-selectivity SIR-based dual-band BPF—fourth-order example—are shown in Fig. 1(a). As can be seen, it consists of a conventional parallel-coupled-line SIR-based BPF—second-order dual-band BPF without TZs—with selectivity-enhancement cells that are internally connected at one node—previously in open circuit—of the input and output coupled-line stages. These one-port cells are made up of two transmission-line segments that are ended in an open circuit at one edge and interconnected at

Manuscript received March 30, 2019; revised May 3, 2019; accepted May 8, 2019. Date of publication June 3, 2019; date of current version July 3, 2019. This work was supported in part by the Spanish Ministry of Economy, Industry, and Competitiveness (State Research Agency) under Project TEC2017-82398-R and in part by the National Science Foundation under Award 1731956. *(Corresponding author: Roberto Gómez-García.)*

R. Gómez-García, L. Yang, and J.-M. Muñoz-Ferreras are with the Department of Signal Theory and Communications, University of Alcalá, Polytechnic School, 28871 Madrid, Spain (e-mail: roberto.gomez.garcia@ieee.org; li.yang@uah.es; jm.munoz@uah.es).

D. Psychogiou is with the Department of Electrical, Computer, and Energy Engineering, University of Colorado Boulder, Boulder, CO 80309 USA (e-mail: dimitra.psychogiou@colorado.edu).

Color versions of one or more of the figures in this paper are available online at http://ieeexplore.ieee.org.

Digital Object Identifier 10.1109/LMWC.2019.2916458

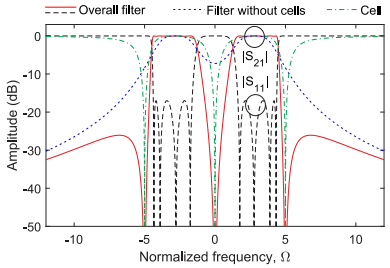

Fig. 2. Theoretical power transmission ($|S_{21}|$) and reflection ($|S_{11}|$) responses of a synthesized example of the coupling–routing diagram in Fig. 1(b) and theoretical $|S_{21}|$ of its cell in transmission mode and of the coupling–routing diagram without cells, i.e., SIR part [$\Omega_1 = -3$, $\Omega_2 = 3$, $\Omega_z = -\Omega_{z1} = \Omega_{z3} = 5$, $\Omega_{z2} = 0$, $J_A \triangleq J_{1,2} = J_{1,4} = J_{9,12} = J_{11,12} = 1.1579$, $J_B \triangleq J_{1,3} = J_{10,12} = 1.2281$, $J_{1,5} = J_{1,7} = J_{6,12} = J_{8,12} = 1.0108$, and $J_{5,6} = J_{7,8} = 0.9147$; note that the design condition (1) is satisfied].

the other one, so that they generate TZs at both sides of the two passbands and increase their order by two. As a result, a higher selectivity dual-band filtering transfer function is realized in the overall filter when compared to its SIR part, i.e., filter without cells. The associated normalized coupling–routing diagram of the devised enhanced-selectivity dual-band BPF is depicted in Fig. 1(b). As observed, the input–output selectivity-enhancement dual-band cells are modeled with three resonating nodes respectively tuned at the normalized TZ frequencies Ω_{z1}, Ω_{z2}, and Ω_{z3} ($\Omega_{z1} < \Omega_{z2} < \Omega_{z3}$) which interact with the source/load nodes through separate admittance inverters. The dual inter-TZ poles of these cells are selected to be equal to the normalized dual-resonance frequencies of the SIRs at Ω_1 and Ω_2 ($\Omega_1 < \Omega_2$) so that they contribute to the order increase of the overall dual passbands. For spectrally symmetrical dual-band responses with regard to the inter-band TZ at $\Omega_{z2} = 0$, the latter implies that the following design formula must be satisfied [$\Omega_z \triangleq -\Omega_{z1} = \Omega_{z3}$, $J_A \triangleq J_{1,2} = J_{1,4} = J_{9,12} = J_{11,12}$, $J_B \triangleq J_{1,3} = J_{10,12}$, $J_{1,5} = J_{1,7} = J_{6,12} = J_{8,12}$, and $J_{5,6} = J_{7,8}$, where the J variables refer to normalized admittance-inversion constants and the node designation indicated in Fig. 1(b) is considered]

$$\Omega_1, \Omega_2 = \mp \frac{J_B \Omega_z}{\sqrt{2J_A^2 + J_B^2}}. \tag{1}$$

For illustration purposes, Fig. 2 represents the power transmission and reflection responses of a synthesized example of the coupling–routing diagram in Fig. 1(b) that was optimized to exhibit perfectly equiripple fourth-order dual passbands with minimum input–output power-matching levels of 17 dB. For comparison purposes, the transfer functions of the selectivity-enhancement cell in transmission mode and of the coupling-routing diagram without the dual-band cells are also depicted. As can be seen, the selectivity increase in the total dual-band BPF with regard to the one without cells is fully demonstrated.

B. Design Guidelines

Due to its distributed quasi-frequency-periodic nature, the selectivity-enhancement dual-band cell in Fig. 1(a) shaped by the connection at its input terminal of two transmission-line segments ended in an open circuit is capable of generating the TZs at both sides of the two passbands at f_{z1}, f_{z2}, and f_{z3} ($f_{z1} < f_{z2} < f_{z3}$). In order the first and second TZs at f_{z1} and f_{z2} to be controlled by the first and second transmission-line segments, respectively, the following design condition must be imposed for their electrical lengths θ_1 and θ_2 :

$$\frac{\pi}{6} < \theta_2(f_{z1}) < \theta_1(f_{z1}) = \frac{\pi}{2} \tag{2}$$

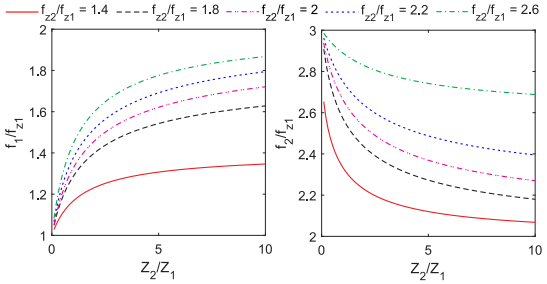

Fig. 3. Normalized-to-f_{z1} theoretical design curves for f_1 and f_2 as a function of Z_2/Z_1 and with f_{z2}/f_{z1} as parameter (note that $f_{z3} = 3f_{z1}$).

so that the relationship below for the TZ frequencies is found

$$0 < f_{z1} < f_{z2} = \frac{\pi f_{z1}}{2\theta_2(f_{z1})} < f_{z3} = 3f_{z1}. \tag{3}$$

At the center frequencies f_1 and f_2 of the one-pole dual-passbands of the dual-band cell produced between the TZs ($f_{z1} < f_1 < f_{z2} < f_2 < f_{z3}$), the input admittances of its transmission-line segments are mutually canceled, that is, $Y_{\text{in}} = 1/Z_{\text{in}} = 0$ in Fig. 1(a). By applying this requisite, the following design equation to obtain f_1 and f_2 is derived

$$\tan\left[\left(\frac{\pi/2}{f_{z2}/f_{z1}}\right)\left(\frac{f}{f_{z1}}\right)\right] = -\frac{Z_2}{Z_1}\tan\left[\frac{\pi}{2}\left(\frac{f}{f_{z1}}\right)\right]. \tag{4}$$

The previous implicit equation can be solved numerically, so that design curves for the center frequencies of the dual-band cell normalized with regard to the first TZ frequency can be obtained. Various examples of these curves are plotted in Fig. 3 as a function of Z_2/Z_1 and different values of f_{z2}/f_{z1}.

Hence, when connecting the dual-band cell at one internal node of both the input and output coupled-line stages as shown in Fig. 1(a), the following operational properties are satisfied.

- The input impedance Z_{in} of the dual-band cell is equal to zero at the TZ frequencies so that no signal transmission occurs at these frequencies in the cell-loaded input and output coupled-line stages. Thus, TZs at these frequencies are also created in the overall dual-band BPF in Fig. 1(a).
- As proven in [6] for a quasi-elliptic single-band BPF counterpart based on uniform-impedance parallel-coupled half-wavelength resonators and an input single-band selectivity-increase cell, the poles of these cells that load the input and output coupled-line stages are transferred to the overall dual passbands to augment their order.

The design process of the selectivity-enhanced dual-band BPF in Fig. 1(a), which uses the previous design guidelines and final optimization, can be divided into the following steps.

1) Synthesis of the SIR part, i.e., filter without selectivity-enhancement cells, as a low-order approximation to the intended overall transfer function with the same center frequencies and bandwidths for the dual passbands [7]. Thus, maximum achievable dual-band bandwidths for the overall BPF are limited by this SIR structure.
2) Design of the selectivity-enhancement cells by using (2) and (3) and the design graphs in Fig. 3 which were derived from (4) to exhibit the same center frequencies and bandwidths in their dual passbands as those desired for the overall dual-band filtering transmission response.
3) Fine-tuning of the total dual-band BPF topology.

An illustrative symmetrical-bandwidth example of the fourth-order quasi-elliptic-type dual-band BPF shown in Fig. 1(a) has been synthesized using this procedure, whose theoretical power transmission and reflection responses are

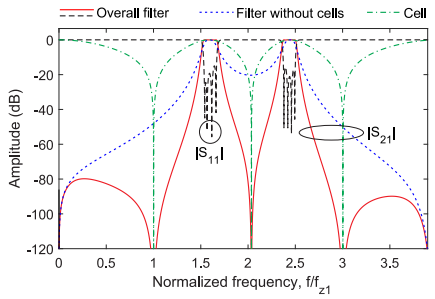

Fig. 4. Theoretical power transmission ($|S_{21}|$) and reflection ($|S_{11}|$) responses of a synthesized example with quasi-equiripple-type passbands of the enhanced-selectivity dual-band BPF in Fig. 1(a) and theoretical $|S_{21}|$ of its cell in transmission mode and of the dual-band BPF without cells, i.e., SIR part ($f_{z2}/f_{z1} = 2.03$, $Z_R = 0.58Z_0$, $Z_{0e1} = 1.64Z_0$, $Z_{0o1} = 0.9Z_0$, $Z_{0e2} = 1.42Z_0$, $Z_{0o2} = 1.18Z_0$, $Z_1 = 0.46Z_0$, $Z_2 = 1.7Z_0$, $\theta_R(f_{z1}) = 41.3^{\circ}$, $\theta_{c1}(f_{z1}) = \theta_{c2}(f_{z1}) = 45.7^{\circ}$, $\theta_1(f_{z1}) = 90^{\circ}$, and $\theta_2(f_{z1}) = 44.3^{\circ}$; Z_0 is the reference impedance).

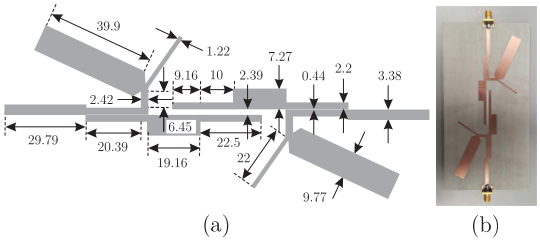

Fig. 5. Manufactured microstrip prototype of SIR-based dual-band BPF with selectivity-enhancement cells (Rogers 4003C substrate: relative dielectric permittivity $\varepsilon_r = 3.38$, dielectric thickness $H = 1.524$ mm, metal thickness $t = 17.8$ μm, and dielectric loss tangent $\tan(\delta_D) = 0.0027$). (a) Layout (dimensions in mm). (b) Photograph.

shown in Fig. 4. Like in the coupling–routing-diagram example shown in Fig. 2, the selectivity improvement attained in the overall filter with regard to the SIR-based part—second-order filter without cells, whose transmission response is also represented—is validated.

III. Experimental Results

To validate the practical usefulness of the proposed SIR-based dual-band BPF with selectivity-enhancement cells, a 50-Ω-referred microstrip prototype has been developed and characterized. It corresponds to the implementation of the fourth-order example shown in Fig. 4 with equal-bandwidth transmission bands located at 1.57 and 2.38 GHz ($f_{z1} =$ 0.98 GHz).

The layout and a photograph of the manufactured microstrip prototype are shown in Fig. 5. Its simulated (with Ansys HFSS) and measured (with a Keysight 5224A network analyzer) power transmission, reflection, and group-delay responses are drawn in Fig. 6. As can be seen, a fairly close agreement between simulated and experimental results is obtained, hence fully validating this filter concept. Note also that, when compared to the simulated transfer function of the filter without the selectivity-enhancement cells, i.e., second-order filter corresponding to the SIR part, which is also depicted, the suppression of the first spurious peak [see Fig. 6(a)] in addition to the improvement of selectivity is to emphasize. The measured characteristics of the constructed dual-band BPF circuit for the lower and upper passbands, respectively, are as follows: center frequencies equal to 1.57 and 2.38 GHz, 3-dB absolute bandwidths of 156 and 156 MHz (i.e., equal to 9.9% and 6.5% in relative terms), minimum in-band power-insertion-loss levels of 1.21 and 1.95 dB, minimum in-band

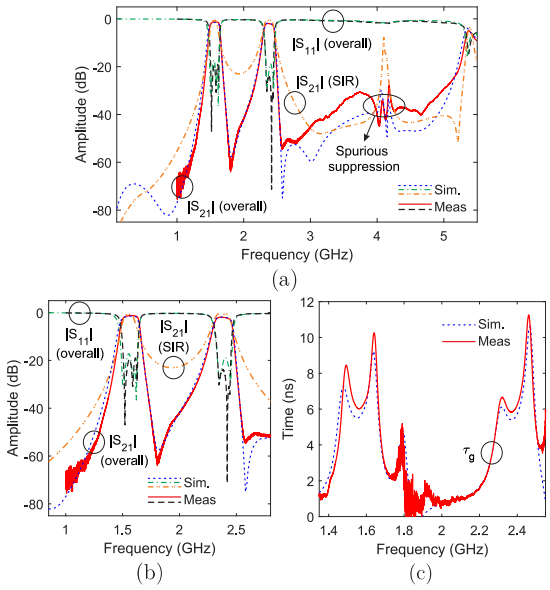

Fig. 6. Simulated and measured power transmission ($|S_{21}|$), reflection ($|S_{11}|$), and group-delay (τ_g) responses of the manufactured microstrip prototype of SIR-based dual-band BPF with selectivity-enhancement cells and simulated $|S_{21}|$ response of its SIR part (i.e., filter without cells). (a) $|S_{21}|$ and $|S_{11}|$ (wideband range). (b) $|S_{21}|$ and $|S_{11}|$ (passband detail). (c) τ_g.

input-power-matching levels—maximum at the ripple—of 19 and 24 dB, and maximum in-band group-delay variations of 4.6 and 5.5 ns. The 25-dB-attenuation-referred upper stopband extends from 2.5 to 5.14 GHz, i.e., 3.27 times the measured lower passband center frequency.

IV. Conclusion

A technique to increase selectivity in SIR-based dual-band BPFs have been presented. It exploits the use of dual-band filtering cells that are internally connected at one node of the input and output coupled-line stages. Thus, two poles are added to the two passbands and stopband TZs are generated at their both sides so that an overall quasi-elliptic-type dual-band filtering transfer function is realized. The theoretical foundations and design rules of the conceived high-selectivity dual-band BPF have been expounded. In addition, a 1.57-GHz/2.38-GHz proof-of-concept microstrip prototype has been developed and tested.

References

[1] J.-M. Yan, L.-Z. Cao, J. Xu, and R.-S. Chen, "Design of a fourth-order dual-band bandpass filter with independently controlled external and inter-resonator coupling," *IEEE Microw. Wireless Compon. Lett.*, vol. 25, no. 10, pp. 642–644, Oct. 2015.

[2] Y.-H. Cho, H.-I. Baek, H.-S. Lee, and S.-W. Yun, "A dual-band combline bandpass filter loaded by lumped series resonators," *IEEE Microw. Wireless Compon. Lett.*, vol. 19, no. 10, pp. 626–628, Oct. 2009.

[3] C. Zhu, J. Xu, G. Zhang, W. Kang, and W. Wu, "Split-type dual-band bandpass filters with symmetric/asymmetric response," *IEEE Microw. Wireless Compon. Lett.*, vol. 28, no. 1, pp. 25–27, Jan. 2018.

[4] R. Gomez-Garcia, J.-M. Munoz-Ferreras, and M. Sanchez-Renedo, "Signal-interference stepped-impedance-line microstrip filters and application to duplexers," *IEEE Microw. Wireless Compon. Lett.*, vol. 21, no. 8, pp. 421–423, Aug. 2011.

[5] C. Quendo, E. Rius, and C. Person, "An original topology of dual-band filter with transmission zeros," in *Proc. IEEE MTT-S Int. Microw. Symp.*, Philadelphia, PA, USA, Jun. 2003, pp. 1093–1096.

[6] C.-J. Chen, "A coupled-line coupling structure for the design of quasi-elliptic bandpass filters," *IEEE Trans. Microw. Theory Techn.*, vol. 66, no. 4, pp. 1921–1925, Apr. 2018.

[7] S. Sun and L. Zhu, "Compact dual-band microstrip bandpass filter without external feeds," *IEEE Microw. Wireless Compon. Lett.*, vol. 15, no. 10, pp. 644–646, Oct. 2005.